AGU
ADVANCING EARTH AND SPACE SCIENCES

Geophysical Research Letters®

Key Points:
- The shallow opening of an ocean gateway leads to an abrupt onset of a deep-reaching overturning circulation
- The deep-reaching overturning circulation is a consequence of standing meanders allowing for full-depth vertical heat transport
- Further deepening of the gateway leads to a weaker overturning due to a decrease in heat transport toward southern convection regions

Supporting Information:
Supporting Information may be found in the online version of this article.

Correspondence to:
Q. Xing,
qianjiang.xing@utas.edu.au

Author Contributions:
Formal analysis: Qianjiang Xing, David Munday
Funding acquisition: Andreas Klocker, David Munday, Joanne Whittaker
Investigation: Qianjiang Xing, Andreas Klocker, David Munday
Methodology: Qianjiang Xing, Andreas Klocker, David Munday
Project Administration: Andreas Klocker, Joanne Whittaker
Supervision: Andreas Klocker, David Munday, Joanne Whittaker
Visualization: Qianjiang Xing
Writing – original draft: Qianjiang Xing

Deepening of Southern Ocean Gateway Leads to Abrupt Onset of a Deep-Reaching Meridional Overturning Circulation

Qianjiang Xing[1] , Andreas Klocker[2] , David Munday[3] , and Joanne Whittaker[1]

[1]Institute for Marine and Antarctic Studies, University of Tasmania, Hobart, TAS, Australia, [2]NORCE Norwegian Research Centre, Bjerknes Centre for Climate Research, Bergen, Norway, [3]British Antarctic Survey, Cambridge, UK

Abstract During the Eocene and the Eocene-Oligocene transition, the lower cell of the meridional overturning circulation (MOC), associated with bottom water formation, underwent changes associated with the geological evolution of Southern Ocean gateways. These are important for the Cenozoic climate transition from Greenhouse to Icehouse, but their dynamics still remain elusive. We demonstrate, using an idealized eddying ocean model, that the opening of a gateway leads to the abrupt onset of a vigorous, deep-reaching, MOC. This MOC has a maximum transport for a shallow gateway, and decreases with further deepening of the gateway. This abrupt change in the MOC can be explained through the ability with which standing meanders—turbulent features located downstream of the gateway—can induce deep vertical heat transport at high latitudes where bottom waters are produced. Our results demonstrate the crucial role of turbulent processes in setting the strength of the global ocean's deep-reaching MOC.

Plain Language Summary Around 50–34 million years ago, the Southern Hemisphere witnessed a major reorganization of continents. This led to the opening and deepening of two Southern Ocean gateways (OGs)—the Tasmanian Gateway between Australia and Antarctica, and Drake Passage between Cape Horn and the Antarctica Peninsula. During this period Earth's climate went through a major climate transition, from a hot world ("Greenhouse") to a cold world ("Icehouse"). One hypothesis to explain this dramatic climate transition is that the opening of these ocean gateways led to a major transition in the ocean's overturning circulation (i.e., its vertical circulation) with important consequences for the ocean's capability to store heat and carbon. In this study we use an ocean model to understand how the opening of an OG affects the ocean's overturning circulation. We show that it is small-scale processes, and their ability to transport heat southward and downward, which lead to a sudden increase of the ocean's overturning circulation as soon as the OG opens. Further deepening of the ocean gateways then leads to a decrease in the overturning circulation. This study therefore highlights the crucial role of small-scale processes in changing Earth's climate.

1. Introduction

The long-term investigation into the meridional overturning circulation (MOC) is primarily motivated by its prominent role in the global redistribution of heat and cycling of chemical elements (Cessi, 2019; Kuhlbrodt et al., 2007; Talley, 2013). In the widely accepted paradigm, the modern MOC is composed of an upper cell, associated with the formation of North Atlantic Deep Water (NADW) in the North Atlantic and the Nordic Seas, and a lower MOC cell, associated with the formation of Antarctic Bottom Water (AABW) around the Antarctic coast (G. C. Johnson, 2008; H. L. Johnson et al., 2019; Marshall & Speer, 2012). The initiation of the modern MOC can be traced to the Eocene-Oligocene transition (EOT, ~34 Ma) (Boyle et al., 2017; Ferreira et al., 2018; Hohbein et al., 2012; Hutchinson et al., 2021; Thomas et al., 2014). Before this time, throughout the Paleocene and early Eocene (~65–40 Ma), geological evidence point toward a bipolar mode of the MOC in the Pacific basin, with deepwater formation occurring both in the North Pacific and the Southern Ocean (Hague et al., 2012; Thomas, 2004; Thomas et al., 2014). Model simulations propose a mode in which deepwater formation occurs only in the Southern Ocean (Y. Zhang et al., 2020, 2022).

These large changes in the MOC are thought to have been triggered by tectonic changes, involving the opening and deepening of the ocean gateways, such as Greenland-Scotland Ridge and Southern Ocean gateways (Abelson & Erez, 2017; Borrelli et al., 2014; Hutchinson et al., 2021; Katz et al., 2011). The deepening of Drake Passage (DP), for example, is thought to have led to deep water upwelling in the Southern Ocean driven by wind stress, closing the modern MOC (Sijp & England, 2004; Toggweiler & Bjornsson, 2000). While many studies focus on

understanding changes in the MOC between fully open and fully closed gateways, recent work has shown how a progressive deepening of DP affects the global MOC (Toumoulin et al., 2020). Before the opening of DP, southern sinking, associated with the lower MOC cell, occurs in the Atlantic basin and is constrained to shallow depth (Toumoulin et al., 2020). After the opening of DP to 100 m depth, southern sinking partially shifts to the Pacific, and the lower MOC cell abruptly strengthens to almost twice modern values, but weakens for a further gateway deepening (Toumoulin et al., 2020). These simulations, showing the effect of the progressive deepening of DP on the MOC, have been run with a complex Earth System model with a coarse-resolution ocean, and hence turbulent processes, such as mesoscale eddies, need to be parameterized. As such, it is difficult to pin down the exact ocean dynamics leading to this radical change in the MOC.

The deepening of ocean gateways forms large local bathymetric features, such as ridges and seamounts. These bathymetric features have profound effects on the dynamics of the Antarctic Circumpolar Current (ACC), generating Rossby waves due to jets in the ACC interacting with them. Rossby waves propagate westward against the ACC mean flow (C. W. Hughes, 2005; X. Zhang et al., 2023). When their propagation speed matches the speed of the eastward-flowing ACC, these Rossby waves become standing Rossby waves, also known as standing meanders (C. W. Hughes, 2005). Mathematically, standing meanders can be presented as time-mean deviations from the zonal-mean component of the ACC (Ivchenko et al., 1996; Youngs et al., 2017). Standing meanders in the modern ACC influence heat transport and closure of the overturning circulation (Youngs et al., 2017). For example, hot spots of eddy heat flux along the ACC occur around major bathymetric features where standing meanders occur. This indicates that they may contribute to strong poleward heat transport across the ACC (Foppert et al., 2017). However, the role of standing meanders during gateway deepening, such as that during the EOT, is uncertain since coarse-resolution ocean models used in these studies do not resolve these turbulent processes, and it is unclear how well parameterizations of these processes work.

In this work, we use an idealized sector model to understand the role of gateway deepening on the evolution of the lower MOC cell. The model domain is that of a narrow sector with a blocked ocean basin, such as the Atlantic basin, to the north, and a zonally re-entrant channel, such as the Southern Ocean, to the south. Due to the limited size of the domain, it is possible to use a horizontal resolution that allows for the representation of mesoscale eddies, whilst remaining computationally efficient. This allows for the long spinup necessary to achieve statistical equilibrium. This work builds on results of Klocker et al. (2023), who used the same model configuration, but with only a fully closed and fully open ocean gateway (OG). Their aim was to understand how buoyancy forcing alone can generate a deep-reaching two-cell MOC, similar to that observed. We use this configuration to analyze changes in ocean dynamics when we introduce different gateway depths to the model geometry. We seek to answer the following two questions based on Toumoulin et al.'s simulation—why does the initial opening of the OG generate a vigorous lower MOC cell?, and why does the simulated lower MOC cell weaken with the deepening of OG? Using these idealized eddying simulations allows us to understand the role of eddies and standing meanders on the lower MOC cell, and to test if the parameterizations used in coarse-resolution Earth System Models reproduce these processes adequately. Note also that while several other ocean gateways have been shown to lead to major changes in the MOC, such as the Central American Seaway and Arctic gateways, we will here focus purely on the effect of a Southern OG and its influence on the lower MOC cell.

2. Methods

2.1. Model and Simulations

The model configuration is based on an ocean-only sector model domain using the Massachusetts Institute of Technology general circulation model (MITgcm) (Marshall, Adcroft, et al., 1997; Marshall, Hill, et al., 1997). As shown in Figure 1, the model domain is composed of an ocean basin extending from 60°S to 60°N, and 0°E–20°E. An OG is located in the latitudes of 60°S–40°S. We refer to the OG as "OG" for the sake of convenience. The model domain has 1/6° horizontal grid spacing, allowing for mesoscale eddies (Note that no mesoscale eddy parameterization used). There are 42 unevenly spaced vertical levels with a 10 m thickness at the surface level, stretching to 250 m at the bottom, for a total depth of 5000 m. At the surface, temperature is restored to a fixed distribution, with a restoring time scale of 10 days. The sea surface temperature at the equator is restored to 30°C, the southern end of the domain to 0°C, and the northern end of the domain to 5°C. A linear equation of state is used for density with a constant salinity of 35 psu. There is no wind forcing or other mechanical forcing. The background vertical diffusivity is set to $K_v = 10^{-6}$ m^2 s^{-1}. More details of the model configuration can be found in Klocker et al. (2023).
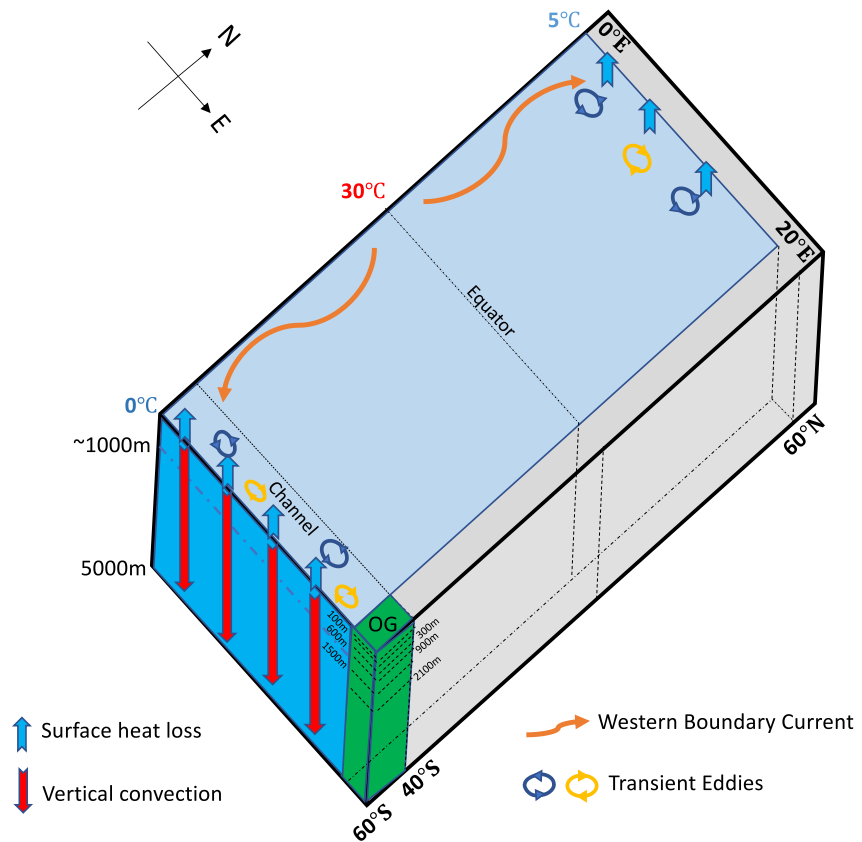
Figure 1. Schematic of model domain and ocean circulation. The domain ranges from 0°E to 20°E and 60°S–60°N. Orange curved arrows indicate western boundary currents. In the channel (60°S–40°S), colored circles are transient eddies, blue vertical arrows are surface heat loss. Red vertical arrows at the southern end indicate vertical convection along the southern boundary.

Experiments with both a fully closed OG (*OG_closed*), and a fully open OG (*OG_open*), were run for 3000 model years in Klocker et al. (2023). Based on these two existing cases, we conduct six sensitivity experiments in which we change the OG depth (the depth of the OG topography beneath sea surface) to 100 m (*OG_100*), 300 m (*OG_300*), 600 m (*OG_600*), 900 m (*OG_900*), 1500 m (*OG_1500*), and 2100 m (*OG_2100*). We run all six sensitivity experiments for 2500 model years from the *OG_closed* case, and use the final 50 years for our analysis.

2.2. Calculation of the Meridional Overturning Circulation

To accurately describe the MOC, composed of horizontal and vertical flows along and across density surfaces, it is necessary to calculate the MOC in density coordinates (Döös & Webb, 1994). We calculate the meridional transport (*VH*) between every density layer, where *V* is meridional velocity and *H* is thickness of density layer. We take the vertical integral of *VH*, then zonally integral and finally average over time to get the total MOC in density coordinates (Ballarotta et al., 2013). This is defined as

$$\Psi^{\sigma}_{total} = \frac{1}{t_1 - t_0} \int_{t_0}^{t_1} \int_{x_W}^{x_E} \sum_{z^s_{\sigma}(\sigma)}^{z^b_{\sigma}(\sigma)} V H \, dx \, dt. \tag{1}$$

Here x_W and x_E are the longitudes of the western and eastern boundaries of the model domain, z^s_{σ} and z^b_{σ} are surface and bottom density layer, and t_0 and t_1 are the start and end point of the time average, respectively. Note that the vertical sum in Equation 1 is vertically accumulation in density bins.

We then use the thickness of density layers $(z_{\sigma}(\sigma))$ and the time-average density distribution in depth coordinates $(\sigma(x, y, z))$ to linearly interpolate the density-coordinate MOC on to depth coordinates.

2.3. Calculation of Meridional Heat Transport and Vertical Heat Transport

The zonally integrated meridional heat transport (*MHT*) is calculated on each depth level as

$$MHT = \frac{\rho_0 C_\rho}{t_1 - t_0} \int_{t_0}^{t_1} \int_{x_W}^{x_E} VT \, dx, \tag{2}$$

where V is zonal velocity, T is potential temperature, ρ_0 the reference density, and C_ρ is the specific heat capacity. When zonally and vertically integrating the MHT, we get

$$MHT_Z = \frac{\rho_0 C_\rho}{t_1 - t_0} \int_{t_0}^{t_1} \int_{x_W}^{x_E} \int_{z_b}^{z_s} VT \, dz \, dx \, dt, \tag{3}$$

where z^s and z^b are the surface and bottom layer.

The vertical heat transport (*VHT*) is calculated by horizontally integrating the vertical advective flux of potential temperature at each depth level,

$$VHT = \frac{\rho_0 C_\rho}{t_1 - t_0} \int_{t_0}^{t_1} \int_A WT \, dA \, dt, \tag{4}$$

where W is the vertical velocity and A is horizontal area of the ocean domain.

2.4. Decomposition Into Eddy, Standing-Meander, and Mean Components

We can use Reynolds averaging to decompose the total transport of any tracer, such as temperature, into its mean, eddy, and standing meander components (Vallis, 2017). The times and zonal averages operate on the product of meridional velocity and temperature in Equation 3. This produces three terms, since the covariance of V and T is non-zero by construction. We can then decompose the total MHT_Z into three components:

$$MHT_Z = \rho_0 C_\rho \int_{x_W}^{x_E} \int_{z_b}^{z_s} \left[\langle \overline{V} \rangle \langle \overline{T} \rangle + \overline{V^* T^*} + \overline{V' T'} \right] dz \, dx, \tag{5}$$

where the first term of right side is mean flow component $\left(\langle \overline{MHT} \rangle_Z \right)$, the second term is the standing meander component $\left(MHT_Z^* \right)$, and the third term is transient eddy component $\left(MHT_Z' \right)$. Similarly, we use this decomposition for the VHT, giving $\langle \overline{VHT} \rangle$, *VHT** and *VHT'*.

3. Results

3.1. Overturning Circulation With Fully Open and Fully Closed Gateway

Due to the heating of the ocean surface at the equator and cooling at high latitudes, ocean circulation adjusts to allow for a heat transport from the equator to high latitudes through a process known as (rotating) horizontal convection (Gayen & Griffiths, 2022; G. O. Hughes & Griffiths, 2008). In a closed basin, such as in experiment *OG_closed*, meridional boundaries allow for the generation of an east-west pressure gradient, and hence the poleward heat transport is due to western boundary currents (WBCs) associated with ocean gyres (Figure S1b in Supporting Information S1). These WBCs transport heat poleward very efficiently and lead to a shallow MOC (Figure 2a), consistent with previous results (Klocker et al., 2023).

In the absence of meridional boundaries, such as in experiment *OG_open*, WBCs cannot exist in the latitude range of the channel (Figure S1j in Supporting Information S1). At these latitudes only turbulent processes, such as mesoscale eddies, can transport heat across the channel (Figures 4i and 4j). These mesoscale eddies are generated by baroclinic instability due to steeply sloping density surfaces across the channel. These surfaces also generate a circumpolar current, resembling the ACC (Figure S1i in Supporting Information S1), via thermal wind balance. As shown by Klocker et al. (2023), the presence of eddies allows for a deep-reaching MOC, as opposed to the shallow MOC observed in the presence of meridional boundaries. In experiment *OG_open*, the surface buoyancy forcing generates a lower MOC cell with a strength (T_{MOC}) of 0.89 Sv, which is equivalent to 16.02 Sv when extrapolated from the width of the sector model to the full width of the ocean (Figures 2h and 2i).
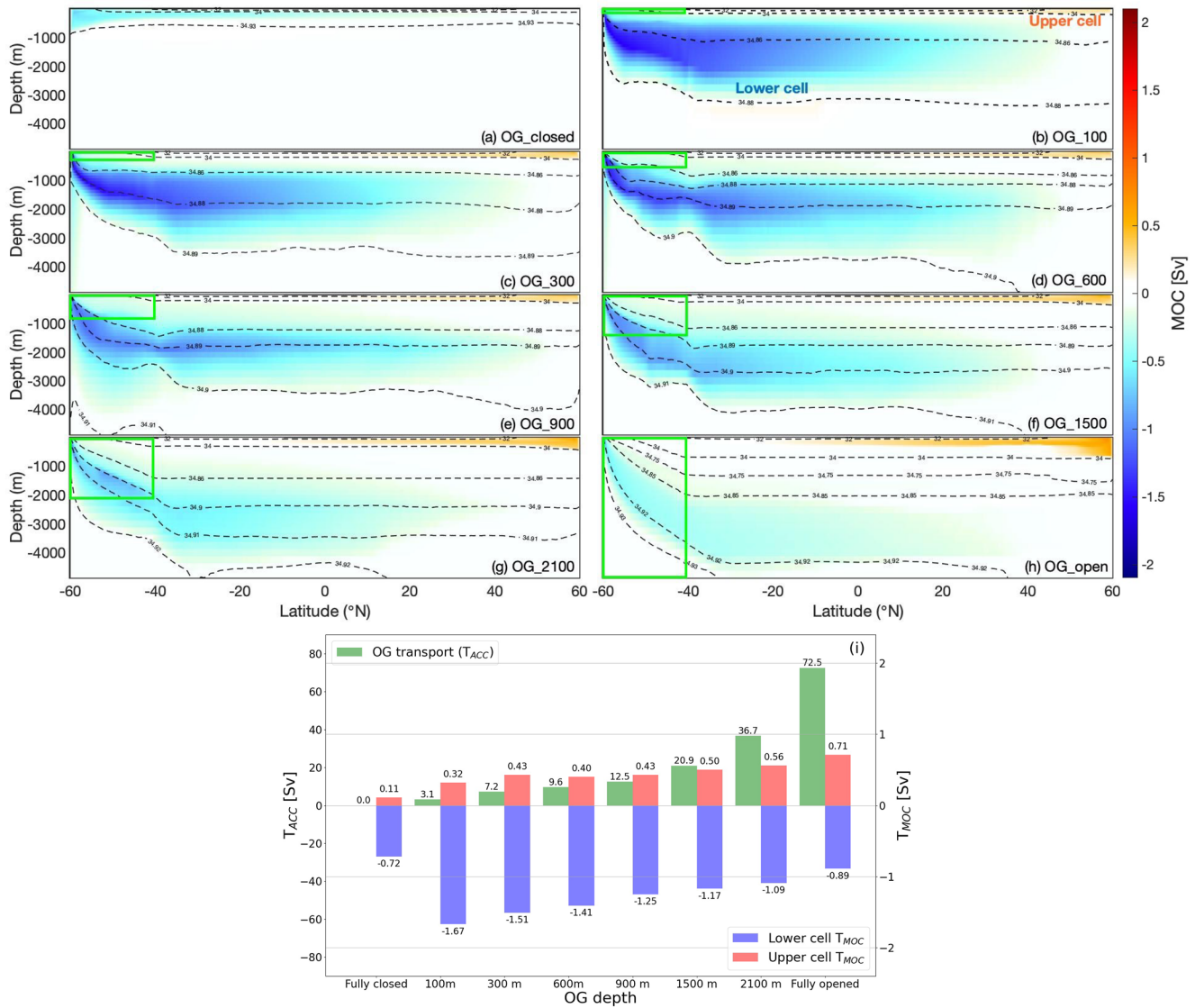
Figure 2. (a–h) Meridional overturning circulation (MOC) (Sv) of all simulations. The upper cell (red) is the clockwise overturning cell, and the lower cell (blue) is the counterclockwise overturning cell. (i) Transport through ocean gateway (OG) (T_{ACC} [Sv]; green), maximum MOC (T_{MOC} [Sv]) for the upper cell (red) and the lower cell (blue).

For both *OG_closed* and *OG_open*, the MOC is closed by vertical plumes against the northern and southern headwall of the domain (Gayen & Griffiths, 2022; G. Hughes et al., 2007). In these regions, a destabilizing buoyancy flux at the ocean surface leads to the formation of deep and bottom waters (Gayen & Griffiths, 2022). The heat in both cases can be transported by mean flows in the form of WBCs, or by mesoscale eddies across the re-entrant channel to generate an overturning cell. Below we will show that in the cases of partially open gateway there is a third process—standing meanders—which can lead to lateral and VHT, allowing for the formation of a deep-reaching MOC.

3.2. Deep-Reaching Overturning Circulation With Gateway Deepening

A shallow OG, as in experiment *OG_100*, allows the formation of a vertically-sheared circumpolar current (Figure 2i). This circumpolar current is the result of the combination of buoyancy loss at the southern boundary, which, together with the lack of meridional boundaries above the OG depth, leads to the steepening of density surfaces and hence a (weak) associated circumpolar current with a zonal transport (T_{ACC}) of 3.1 Sv (Figure 2i).
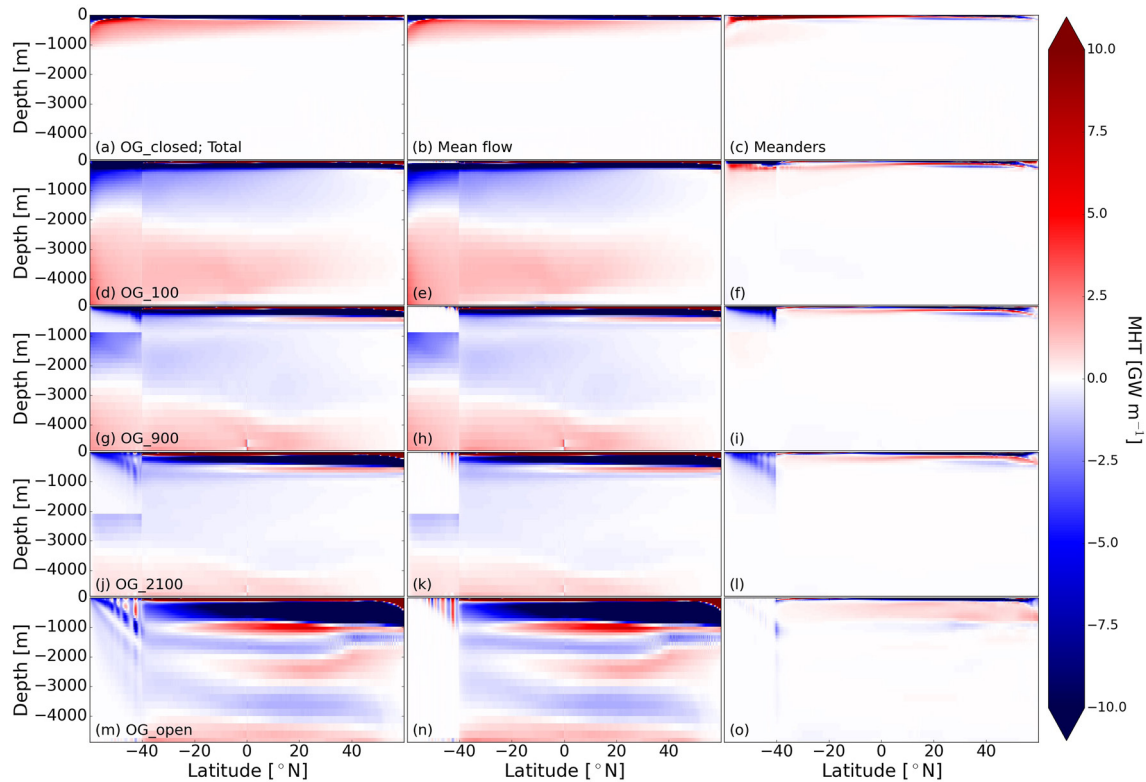
Figure 3. Hydrographic section of the zonally integrated meridional heat transport (*MHT*) (Gigawatt [GW] m⁻¹) for experiments *OG_closed*, *OG_100*, *OG_900*, *OG_2100*, and *OG_open*. Red colors indicate northward heat transport and blue colors indicate southward heat transport. Left panels show total *MHT*, middle panels show the *MHT* by the mean flow $\left(\left\langle \overline{MHT} \right\rangle \right)$, and right panels show the *MHT* by standing meanders (*MHT**). Hydrographic sections of *MHT* in the upper layer (<1000 m) are shown in the Figure S4 in Supporting Information S1.

This circumpolar current is baroclinically unstable, resulting in the generation of transient eddies and standing meanders, with the latter being generated due to the circumpolar current interacting with the topography of the OG.

A striking change is the deep-reaching MOC in *OG_100*, despite the very shallow OG, the lower MOC cell now extends to about 3500 m, and increases from 0.72 Sv in *OG_closed* to 1.67 Sv in *OG_100* (global scale: 30.06 Sv; Figures 2b and 2i). With further deepening of the OG from 100 to 2100 m (experiments *OG_100* to *OG_2100*), the transport of the eastward circumpolar current (T_{ACC}) gradually increases to 36.7 Sv (Figure 2i). In contrast with the increasing transport of the circumpolar current, the lower MOC cell continuously weakens to 1.09 Sv (global scale: 19.62 Sv) for the 2100 m OG experiment (Figure 2i). The shallowest OG therefore leads to the strongest lower MOC cell, with further deepening leading to a reduction in strength of the lower MOC cell. This behavior of the lower overturning cell is consistent with recent results using a complex earth system model (Toumoulin et al., 2020), despite the differences in model grid spacing and complexity.

3.3. The Role of Ocean Heat Transport

Buoyancy (heat) loss (see Figure S3 in Supporting Information S1) at the southern boundary of the channel leads to deep convection (Gayen & Griffiths, 2022) and hence the lower MOC cell (see Figure 1). In an equilibrated ocean, maintaining the buoyancy loss, and a deep-reaching overturning, requires a continuous supply of heat toward the southern ("Antarctic") boundary. The lower MOC cell is accordingly controlled by this heat supply. In this section, we will show how changes in OG depth affect the distribution of meridional and VHT by mean flows, standing meanders, and transient eddies.

For the experiment with a closed OG (*OG_closed*), the zonally integrated MHT is dominated by the mean flow (Figures 3a and 3b), transporting heat southward (blue colors) at the surface and northward (red colors) below
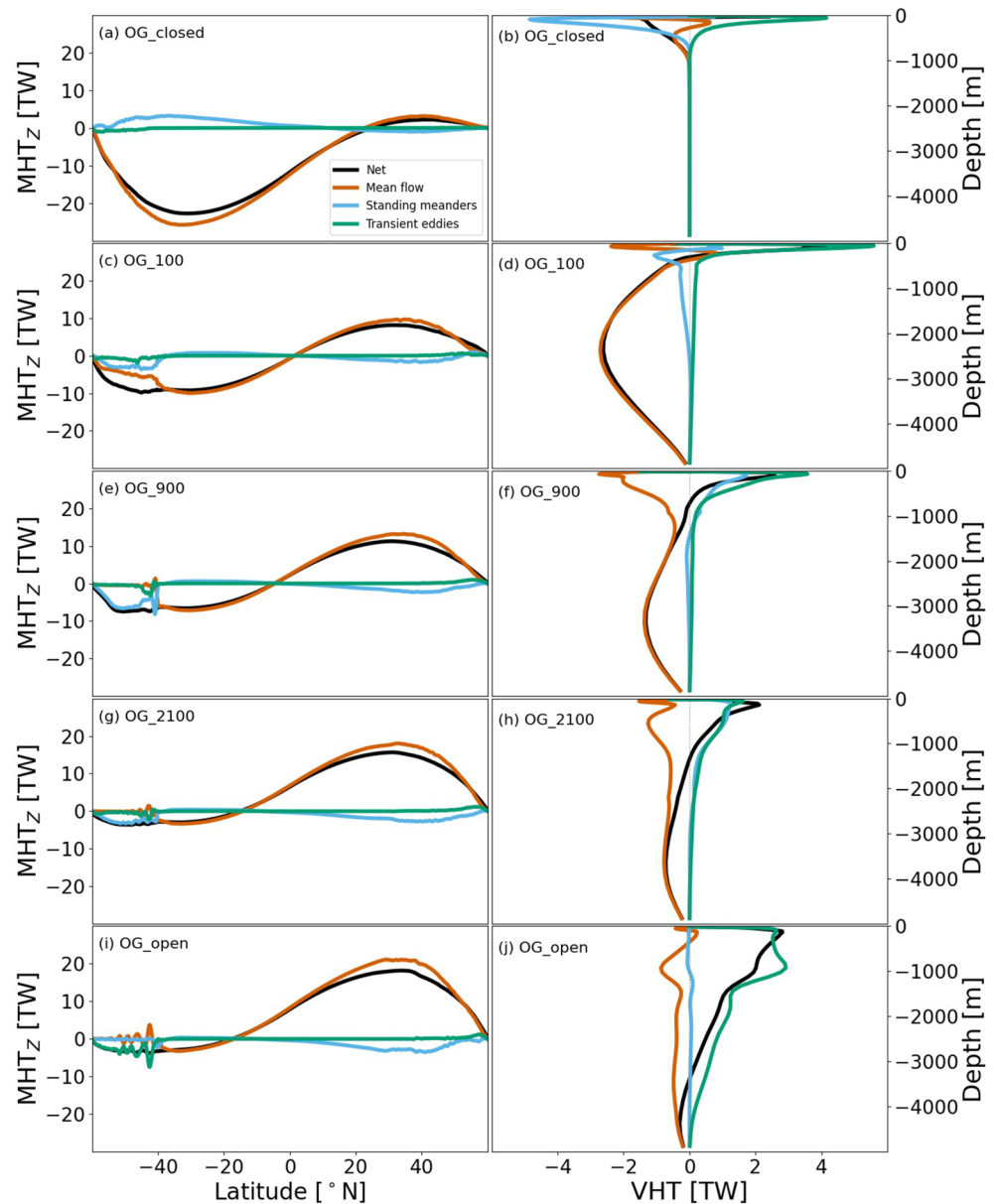
Figure 4. (a, c, e, g, i) Zonally and vertically integrated meridional heat transport (MHT_Z) (Terawatt [TW]) for experiments *OG_closed*, *OG_100*, *OG_900*, *OG_2100*, and *OG_open*. (b, d, f, h, j) Horizontal integrated vertical heat transport (*VHT*) [TW] in the channel for experiments *OG_closed*, *OG_100*, *OG_900*, *OG_2100*, and *OG_open*. See more details about MHT_Z and VHT of all experiments in the Figure S6 in Supporting Information S1. In all panels, black lines indicate the total (MHT_Z, *VHT*), orange lines the mean component ($\langle \overline{MHT} \rangle_Z$, $\langle \overline{VHT} \rangle$), green lines the standing meanders (MHT_Z^*, *VHT**), and blue lines the transient eddies (MHT'_Z, *VHT'*).

(Figure 3b, Figure S4 in Supporting Information S1). This is consistent with the MOC being confined to the shallow ocean, with the deep ocean being largely at rest (Figures 2a and 3a–3c). In the southern part, standing meanders produce a southward MHT (*MHT**) at the surface, and a northward MHT below. Transient eddies lead to a southward MHT across the channel, but contribute less to the heat transport than either the mean flow or standing meanders (Figure S4 in Supporting Information S1). The vertically integrated MHT (MHT_Z) is strongly biased toward the southern high latitudes. This is consistent with experiments of thermally-driven flows in a domain lacking a re-entrant channel, in which the flow is biased toward the pole with the colder temperature forcing (Coman et al., 2010; Figure 4a). Consistent with the shallow confinement of the MHT and MOC, the VHT is confined to the shallow ocean (Figure 4b). In summary, in *OG_closed* the entire heat transport is by baroclinic gyres which are confined to the ocean surface, leading to a shallow MOC. The deep ocean is at rest.

When the OG opens to a depth of 100 m (*OG_100*), the total MHT suddenly extends to the full depth of the basin rather than being confined to the shallow ocean (Figure 3d). This is mainly composed of a southward MHT from surface to mid-depth, and a northward MHT below, both due to the mean component of the flow (Figure 3e). This corresponds to a full-depth lower MOC cell which increases in strength from 0.72 Sv in *OG_closed* to 1.67 Sv. Standing meanders lead to a southward MHT above the OG depth, and a northward MHT below the OG depth (Figure 3f). Transient eddies still provide a weak southward MHT in the channel (Figure S5 in Supporting Information S1). The total vertically and zonally integrated southward MHT $\left(MHT_Z^* \right)$ in the southern half of the basin is reduced by about half, with a maximum of about 10 Terawatt (TW) compared to *OG_closed*. This is due to both the mean flow and standing meanders (Figure 4c). On the other hand, the northward MHT in the northern half of the basin increases by 8 TW compared to *OG_closed*. Transient eddies again provide little MHT $\left(MHT_Z' \right)$ relative to the mean flow and standing meanders. In contrast to the large decrease in MHT by the mean flow in *OG_100*, the VHT by the mean flow shows a large increase in strength and now extends to the full depth (Figure 4d).

For a further OG deepening (from *OG_100* to *OG_2100*), the mean MHT in the deep ocean decreases in strength compared with *OG_100*, reflected by lighter blue and red colors in Figures 3h–3k and Figure S5 in Supporting Information S1. This corresponds to a weakening of the deep-reaching MOC. In the channel, standing meanders lead to a southward MHT above the OG depth (Figure 3). The MHT by transient eddies increases, although it is still weaker than the other terms (Figure S5 in Supporting Information S1). The gradual deepening of the OG strengthens the transport of the circumpolar current, and leads to a state where the vertically integrated MHT is entirely due to standing meanders (Figures 4e and 4g) in the channel. The vertically integrated MHT by standing meanders becomes weaker the deeper the OG, leading to a decrease in strength of the lower MOC cell for a further OG deepening. This weakening of the southward MHT is accompanied by a strengthening of the northward vertically integrated MHT, and hence a stronger upper overturning cell (Figure 2).

When the OG is fully open (*OG_open*), standing meanders cannot exist since their existence relies on the interaction with a ridge, and instead transient eddies provide southward MHT (Figure 3o and Figure S5 in Supporting Information S1). For this experiment the MOC is still full-depth, but weaker than in all cases where standing meanders are present. This experiment therefore shows that eddies are also capable of allowing for a full-depth lower MOC cell. However, given that transient eddies are less efficient at transporting heat toward the southern convection region, the lower MOC cell is weaker than in all cases where standing meanders are present.

4. Discussion and Conclusion

In summary, the evolution of the deep-reaching lower MOC cell with the deepening of the OG can be divided into two parts: the abrupt onset of the deep-reaching lower MOC cell for a shallow OG, and the subsequent weakening for a further deepening of the OG. This behavior of the lower MOC cell is closely linked to changes in southward and downward heat transport in the presence of standing meanders. First, in an equilibrated ocean, the strength of an overturning cell is limited by the amount of heat which can be supplied to the vertical plumes associated with strong surface buoyancy loss. This heat supply is most efficient if mean flows, such as WBCs, are present. This heat supply becomes less efficient if the heat transport is due to standing meanders, and even less efficient if heat supply is due to transient eddies. A deepening OG allows a zonal flow in the channel to gradually block WBCs and induces weakening of subpolar gyres (Sauermilch et al., 2021). As a result, it leads to a reduced heat transport to southern high latitudes, which is compensated with an increased heat transport to northern high latitudes. This northward heat transport may contribute to strengthening the upper MOC cell, associated with the formation of NADW. Second, a deep-reaching overturning cell is dependent on a process which can get this heat to depth. As shown by Klocker et al. (2023), this can be achieved by transient eddies, and, as shown here, this can also be achieved by standing meanders produced by zonal flow interacting with the OG. Nevertheless, heat transport by baroclinic gyres is always confined to the surface, and the presence of mesoscale turbulence, whether transient eddies or standing meanders, is necessary to get this heat to depth, and hence lead to a deep-reaching MOC.

The two-part evolution of the lower MOC cell for a deepening of an OG is therefore a combination of the two roles transient eddies and standing meanders play for ocean heat transport. These dynamics lead to a maximum lower MOC cell for the experiment with the shallowest OG, which is a combination of the domain where the southward heat transport is largest (due to mean flow), while at the same time allowing for a deep-reaching heat transport by mesoscale turbulence (mainly due to standing meanders). Further deepening of the OG leads to a weakening

of the southward heat supply across the channel due to the weakening of the surface WBCs and subpolar gyres (Sauermilch et al., 2021), and a strengthening of the northward heat transport, associated with a strengthening of the upper overturning cell. Once the OG is as deep as the rest of the domain, the southward heat transport is solely due to transient eddies, resulting in the weakest deep-reaching overturning cell. As opposed to studies which focus on just fully open and fully closed OGs, we highlight the importance of the dynamics of standing meanders in understanding the evolution of the MOC with gateway deepening. These standing meanders are a turbulent process which is generally neglected in the paleoceanography community due to high computational cost of resolving these small-scale processes. Nevertheless, at least in the results of Toumoulin et al. (2020), the MOC resulting from a deepening of an OG gives similar results to our eddying idealized simulations, giving some hope that parameterizations of these small-scale processes work appropriately.

This study has shown that the strength of the lower MOC cell is highly dependent on Southern OG opening/deepening. It has highlighted the vital contribution of turbulent processes in the MOC evolution during the Eocene and the EOT. Considering the crucial role of MOC system in the redistribution of global heat and carbon, this study sheds light on how the MOC evolves during different climatic transitions and its impact in contributing to a climatically changing world. Future work is planned to extend this work to elucidating the whole story of the global MOC across the early Cenozoic with a global high-resolution ocean model and realistic paleo-bathymetry.

Data Availability Statement

All model output used in this study to perform the analysis and produce figures is available at https://doi.org/10.5281/zenodo.7602996.

References

Abelson, M., & Erez, J. (2017). The onset of modern-like Atlantic meridional overturning circulation at the Eocene-Oligocene transition: Evidence, causes, and possible implications for global cooling. *Geochemistry, Geophysics, Geosystems*, *18*(6), 2177–2199. https://doi.org/10.1002/2017gc006826

Ballarotta, M., Drijfhout, S., Kuhlbrodt, T., & Döös, K. (2013). The residual circulation of the Southern Ocean: Which spatio-temporal scales are needed? *Ocean Modelling*, *64*, 46–55. https://doi.org/10.1016/j.ocemod.2013.01.005

Borrelli, C., Cramer, B. S., & Katz, M. E. (2014). Bipolar Atlantic deepwater circulation in the middle-late Eocene: Effects of Southern Ocean gateway openings. *Paleoceanography*, *29*(4), 308–327. https://doi.org/10.1002/2012pa002444

Boyle, P. R., Romans, B. W., Tucholke, B. E., Norris, R. D., Swift, S. A., & Sexton, P. F. (2017). Cenozoic North Atlantic deep circulation history recorded in contourite drifts, offshore newfoundland, Canada. *Marine Geology*, *385*, 185–203. https://doi.org/10.1016/j.margeo.2016.12.014

Cessi, P. (2019). The global overturning circulation. *Annual Review of Marine Science*, *11*(1), 249–270. https://doi.org/10.1146/annurev-marine-010318-095241

Coman, M., Griffiths, R., & Hughes, G. (2010). The sensitivity of convection from a horizontal boundary to the distribution of heating. *Journal of Fluid Mechanics*, *647*, 71–90. https://doi.org/10.1017/s0022112009993247

Döös, K., & Webb, D. J. (1994). The deacon cell and the other meridional cells of the Southern Ocean. *Journal of Physical Oceanography*, *24*(2), 429–442. https://doi.org/10.1175/1520-0485(1994)024<0429:tdcato>2.0.co;2

Ferreira, D., Cessi, P., Coxall, H. K., De Boer, A., Dijkstra, H. A., Drijfhout, S. S., et al. (2018). Atlantic-Pacific asymmetry in deep water formation. *Annual Review of Earth and Planetary Sciences*, *46*(1), 327–352. https://doi.org/10.1146/annurev-earth-082517-010045

Foppert, A., Donohue, K. A., Watts, D. R., & Tracey, K. L. (2017). Eddy heat flux across the Antarctic circumpolar current estimated from sea surface height standard deviation. *Journal of Geophysical Research: Oceans*, *122*(8), 6947–6964. https://doi.org/10.1002/2017jc012837

Gayen, B., & Griffiths, R. W. (2022). Rotating horizontal convection. *Annual Review of Fluid Mechanics*, *54*(1), 105–132. https://doi.org/10.1146/annurev-fluid-030121-115729

Hague, A. M., Thomas, D. J., Huber, M., Korty, R., Woodard, S. C., & Jones, L. B. (2012). Convection of north Pacific deep water during the early Cenozoic. *Geology*, *40*(6), 527–530. https://doi.org/10.1130/g32886.1

Hohbein, M. W., Sexton, P. F., & Cartwright, J. A. (2012). Onset of North Atlantic deep water production coincident with inception of the Cenozoic global cooling trend. *Geology*, *40*(3), 255–258. https://doi.org/10.1130/g32461.1

Hughes, C. W. (2005). Nonlinear vorticity balance of the Antarctic circumpolar current. *Journal of Geophysical Research*, *110*(C11), C11008. https://doi.org/10.1029/2004jc002753

Hughes, G., Griffiths, R., Mullarney, J., & Peterson, W. H. (2007). A theoretical model for horizontal convection at high Rayleigh number. *Journal of Fluid Mechanics*, *581*, 251–276. https://doi.org/10.1017/s0022112007005630

Hughes, G. O., & Griffiths, R. W. (2008). Horizontal convection. *Annual Review of Fluid Mechanics*, *40*(1), 185–208. https://doi.org/10.1146/annurev.fluid.40.111406.102148

Hutchinson, D. K., Coxall, H. K., Lunt, D. J., Steinthorsdottir, M., De Boer, A. M., Baatsen, M., et al. (2021). The Eocene–Oligocene transition: A review of marine and terrestrial proxy data, models and model–data comparisons. *Climate of the Past*, *17*(1), 269–315. https://doi.org/10.5194/cp-17-269-2021

Ivchenko, V. O., Richards, K. J., & Stevens, D. P. (1996). The dynamics of the Antarctic circumpolar current. *Journal of Physical Oceanography*, *26*(5), 753–774. https://doi.org/10.1175/1520-0485(1996)026<0753:tdotac>2.0.co;2

Johnson, G. C. (2008). Quantifying Antarctic bottom water and North Atlantic deep water volumes. *Journal of Geophysical Research*, *113*(C5), C05027. https://doi.org/10.1029/2007jc004477

Johnson, H. L., Cessi, P., Marshall, D. P., Schloesser, F., & Spall, M. A. (2019). Recent contributions of theory to our understanding of the Atlantic meridional overturning circulation. *Journal of Geophysical Research: Oceans*, *124*(8), 5376–5399. https://doi.org/10.1029/2019jc015330

Katz, M. E., Cramer, B. S., Toggweiler, J., Esmay, G., Liu, C., Miller, K. G., et al. (2011). Impact of Antarctic circumpolar current development on late Paleogene ocean structure. *Science*, *332*(6033), 1076–1079. https://doi.org/10.1126/science.1202122

Klocker, A., Munday, D., Gayen, B., Roquet, F., & LaCasce, J. H. (2023). Deep-reaching global ocean overturning circulation generated by surface buoyancy forcing. *ESS Open Archive*. https://doi.org/10.22541/essoar.169447446.64699431/v1

Kuhlbrodt, T., Griesel, A., Montoya, M., Levermann, A., Hofmann, M., & Rahmstorf, S. (2007). On the driving processes of the Atlantic meridional overturning circulation. *Reviews of Geophysics*, *45*(2). https://doi.org/10.1029/2004rg000166

Marshall, J., Adcroft, A., Hill, C., Perelman, L., & Heisey, C. (1997). A finite-volume, incompressible Navier Stokes model for studies of the ocean on parallel computers. *Journal of Geophysical Research*, *102*(C3), 5753–5766. https://doi.org/10.1029/96jc02775

Marshall, J., Hill, C., Perelman, L., & Adcroft, A. (1997). Hydrostatic, quasi-hydrostatic, and nonhydrostatic ocean modeling. *Journal of Geophysical Research*, *102*(C3), 5733–5752. https://doi.org/10.1029/96jc02776

Marshall, J., & Speer, K. (2012). Closure of the meridional overturning circulation through Southern Ocean upwelling. *Nature Geoscience*, *5*(3), 171–180. https://doi.org/10.1038/ngeo1391

Sauermilch, I., Whittaker, J. M., Klocker, A., Munday, D. R., Hochmuth, K., Bijl, P. K., & LaCasce, J. H. (2021). Gateway-driven weakening of ocean gyres leads to Southern Ocean cooling. *Nature Communications*, *12*(1), 1–8. https://doi.org/10.1038/s41467-021-26658-1

Sijp, W. P., & England, M. H. (2004). Effect of the Drake Passage Throughflow on global climate. *Journal of Physical Oceanography*, *34*(5), 1254–1266. https://doi.org/10.1175/1520-0485(2004)034<1254:eotdpt>2.0.co;2

Talley, L. D. (2013). Closure of the global overturning circulation through the Indian, Pacific, and Southern Oceans: Schematics and transports. *Oceanography*, *26*(1), 80–97. https://doi.org/10.5670/oceanog.2013.07

Thomas, D. J. (2004). Evidence for deep-water production in the North Pacific Ocean during the early Cenozoic warm interval. *Nature*, *430*(6995), 65–68. https://doi.org/10.1038/nature02639

Thomas, D. J., Korty, R., Huber, M., Schubert, J. A., & Haines, B. (2014). Nd isotopic structure of the Pacific Ocean 70–30 ma and numerical evidence for vigorous ocean circulation and ocean heat transport in a greenhouse world. *Paleoceanography*, *29*(5), 454–469. https://doi.org/10.1002/2013pa002535

Toggweiler, J., & Bjornsson, H. (2000). Drake Passage and palaeoclimate. *Journal of Quaternary Science: Published for the Quaternary Research Association*, *15*(4), 319–328. https://doi.org/10.1002/1099-1417(200005)15:4<319::aid-jqs545>3.0.co;2-c

Toumoulin, A., Donnadieu, Y., Ladant, J.-B., Batenburg, S., Poblete, F., & Dupont-Nivet, G. (2020). Quantifying the effect of the Drake Passage opening on the Eocene ocean. *Paleoceanography and Paleoclimatology*, *35*(8), e2020PA003889. https://doi.org/10.1029/2020pa003889

Vallis, G. K. (2017). *Atmospheric and oceanic fluid dynamics*. Cambridge University Press. Chap. 11.1.1.

Youngs, M. K., Thompson, A. F., Lazar, A., & Richards, K. J. (2017). ACC meanders, energy transfer, and mixed barotropic–baroclinic instability. *Journal of Physical Oceanography*, *47*(6), 1291–1305. https://doi.org/10.1175/jpo-d-16-0160.1

Zhang, X., Nikurashin, M., Peña-Molino, B., Rintoul, S. R., & Doddridge, E. (2023). A theory of standing meanders of the Antarctic circumpolar current and their response to wind. *Journal of Physical Oceanography*, *53*(1), 235–251. https://doi.org/10.1175/JPO-D-22-0086.1

Zhang, Y., de Boer, A. M., Lunt, D. J., Hutchinson, D. K., Ross, P., van de Flierdt, T., et al. (2022). Early Eocene ocean meridional overturning circulation: The roles of atmospheric forcing and strait geometry. *Paleoceanography and Paleoclimatology*, *37*(3), e2021PA004329. https://doi.org/10.1029/2021PA004329

Zhang, Y., Huck, T., Lique, C., Donnadieu, Y., Ladant, J.-B., Rabineau, M., & Aslanian, D. (2020). Early Eocene vigorous ocean overturning and its contribution to a warm Southern Ocean. *Climate of the Past*, *16*(4), 1263–1283. https://doi.org/10.5194/cp-16-1263-2020